Heliyon 10 (2024) e30623

Contents lists available at ScienceDirect

Heliyon

journal homepage: www.cell.com/heliyon

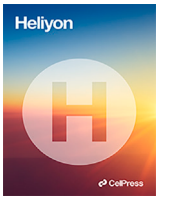

Research article

Measuring the viscoelastic relaxation function of cells with a time-dependent interpretation of the Hertz-Sneddon indentation model

I.V.M. Lima [a], A.V.S. Silva [a,d], F.D. Sousa [c], W.P. Ferreira [a], R.S. Freire [b], C.L.N. de Oliveira [a], J.S. de Sousa [a,*]

[a] Departamento de Física, Universidade Federal do Ceará, Fortaleza, 60440-900, Ceará, Brazil
[b] Central Analítica, Universidade Federal do Ceará, Fortaleza, 60440-900, Ceará, Brazil
[c] Núcleo de Biologia Experimental, Universidade de Fortaleza, Fortaleza, 60811-905, Ceará, Brazil
[d] Instituto Federal do Rio Grande do Norte, Pau dos Ferros, 59900-000, Rio Grande do Norte, Brazil

ARTICLE INFO

Keywords:
Atomic force microscopy
Cell viscoelasticity
Viscoelastic force model
Hertz-Sneddon contact model

ABSTRACT

The Hertz-Sneddon elastic indentation model is widely adopted in the biomechanical investigation of living cells and other soft materials using atomic force microscopy despite the explicit viscoelastic nature of these materials. In this work, we demonstrate that an exact analytical viscoelastic force model for power-law materials, can be interpreted as a time-dependent Hertz-Sneddon-like model. Characterizing fibroblasts (L929) and osteoblasts (OFCOLII) demonstrates the model's accuracy. Our results show that the difference between Young's modulus E_Y obtained by fitting force curves with the Hertz-Sneddon model and the effective Young's modulus derived from the viscoelastic force model is less than 3%, even when cells are probed at large forces where nonlinear deformation effects become significant. We also propose a measurement protocol that involves probing samples at different indentation speeds and forces, enabling the construction of the average viscoelastic relaxation function of samples by conveniently fitting the force curves with the Hertz-Sneddon model.

1. Introduction

Atomic force microscopy (AFM) has become ubiquitous in the rheological characterization of soft matter, particularly in the nanomechanics of living cells [1–7]. The success of the AFM is in part due to its high spatial resolution, precise force control up to a few nano newtons, and ability to probe cells in liquid, but also because that the measured force curves are easily modeled with the well-known Hertz-Sneddon's (HS) model, that describes the axisymmetric indentation of semi-infinite elastic materials [8].

Although soft materials always exhibit some degree of viscoelasticity, the HS model successfully described qualitatively many interesting microscopic phenomena by comparing the mechanical properties of materials with a reference sample measured with identical loading conditions. For instance, a large volume of AFM studies reported that individual cancer cells are less rigid than their normal counterparts [3,9–12], and the same trend was also observed comparing normal and cancerous tissues of the human breast [13]. Beyond cancer, other diseases like osteoarthritis [14,15], tissue fibrosis [16,17] and myocardial infarction [18] exhibit

* Corresponding author.
E-mail address: jeanlex@fisica.ufc.br (J.S. de Sousa).

https://doi.org/10.1016/j.heliyon.2024.e30623
Received 6 February 2024; Received in revised form 15 April 2024; Accepted 30 April 2024

Available online 8 May 2024

distinguished mechanical signatures, which can be used as an advantageous technique to develop early diagnosis methods. More recently, a few works reported the strong role the microenvironment topography plays in cell mechanics. For instance, it was shown that kidney cancer cells become stiffer than normal ones when seeded over soft gels [19] and that cells become softer when crawling in narrow channels [20]. All those studies fitted AFM force curves with the HS model.

Despite those successful advances in the frontier of cell biophysics, nanomechanics has yet to evolve to become a standard metrology-grade characterization because measured data among different studies on the same cells exhibit large dispersion, even in the case where studies use nearly the same measurement parameters and techniques. In the particular case of living cells, this wide dispersion is often attributed to inhomogeneities in the constitution of a biological specimen, variability of sample thickness, differences in sample preparation, and different probing conditions (e.g., maximum applied forces, indentation velocities, indenter geometry). Even the contact point detection in the force curve analysis may impact the mechanical data of cells [21,22]. In this regard, Pérez-Domínguez et al. [23] proposed the standardized operational protocol (SOP), which allows the detection of the biomechanical properties of living cells regardless of the nanoindentation instruments used (AFMs and other indenters) and across laboratories with reproducible mechanical characterization of cells.

Measuring the mechanical properties of cells with the AFM requires careful choice of parameters like cantilever stiffness, tip geometry, applied forces and measurement speeds [24–27]. Tip geometry is important because it defines the contact area and ultimately the spatial resolution of the measurements [24,25]. The maximum applied forces also matter because it is well known that cells may respond non-linearly exhibiting either stress softening or stiffening [26,28], and the speed of measurements is relevant because of the viscoelastic response of cells [26,27]. Despite all these intricacies, most body of knowledge about cell mechanics has been learned within the simple framework of the HS indentation model.

In this work, we show that the HS model can describe force curves of viscoelastic materials, particularly those obeying single power-law viscoelastic relaxation (e.g., living cells). In contrast, the time dependence of the elasticity modulus is encoded in the loading time of the force curve, and that the underlying viscoelastic relaxation function of cells can be constructed with the HS model by simply making several AFM measurements for varying cantilever speeds.

2. Experimentals

Cell culture. The cell lines studied in this work are: L929 (fibroblasts) and OFCOLII (osteoblasts). Cells were grown in high-glucose Dulbecco's Modified Eagle's Medium (GIBCO, USA) supplemented with 10% fetal bovine serum (GIBCO, USA) and 1% penicillin-streptomycin, and incubated at 37^o C in 5% CO_2. Before AFM measurements, one third of medium was replaced by PBS solution to keep pH stable out of the incubator.

AFM measurements. Regular AFM force curves were measured in an Asylum MFP3D-BIO coupled to an inverted optical microscope Nikon IX51. We used AFM cantilevers with nominal spring constant of 0.06 N/m with pyramidal tip (PNP-TR-Au, NanoWorld, with nominal height of 3.5 μm). The maximum force F_{max} applied to the cells ranged between 1 nN and 8 nN to assess nonlinear viscoelastic regimes. The maximum indentation depths ranged between 0.8 μm and 2.0 μm. A piezo extension range (z_{ramp}) of 3 μm was used in all measurements. The indentation speed is controlled by tuning the vertical frequency f_z (0.25 Hz − 2.0 Hz), resulting in cantilever velocities ranging from 1.5 μm/s to 12 μm/s. The force measurements were performed at room temperature (25^o C) in nearly identical conditions. All AFM experiments were performed within two hours after cells were removed from CO_2 incubator.

3. Modeling

3.1. HS model

The analysis of AFM force curves is commonly performed with the HS indentation model given by:

$$F_{el} = \Omega(\lambda) E_Y \delta^{\lambda}, \tag{1}$$

where F_{el} is the force applied by an axisymmetric indenter that produces an indentation depth δ in an elastic medium with Young's modulus E_Y. The parameters $\Omega(\lambda)$ and λ depend on the indenter geometry as listed in Table 1. The HS model assumes that (i) the sample is a purely elastic half-space, (ii) the stress-strain response is linear, and (iii) the elasticity modulus is constant.

Conventional AFM force curves are represented either by a function $F(z)$ or $d(z)$, where $z(t)$ is the piezo displacement and $d(t)$ is the cantilever deflection. The force $F(t)$ on the cantilever is given by $F(t) = k_c(d(t) - d_0)$, where k_c is the cantilever spring constant. The indentation depth of the AFM tip in the sample is determined by $\delta(t) = (z(t) - z_0) - (d(t) - d_0)$, where (z_0, d_0) is the contact point, i.e., the piezo displacement and cantilever deflection at the moment that the AFM tip touches the sample surface. By assuming that the AFM tip is in equilibrium during the whole indentation process, one combines the above equations to obtain

$$k_c(d - d_0) = \Omega_\lambda E_Y [(z - z_0) - (d - d_0)]^{\lambda}, \tag{2}$$

where the time dependence in $z(t)$ and $d(t)$ was omitted by convenience. This is the most used expression to fit AFM force curves, whose fitting parameters are E_Y, z_0 and d_0. It is known that a poor detection of (z_0, d_0) may influence the determination of E_Y [21]. In this regard, several strategies to determine the contact point were developed [22,29]. We employed Roy et al. bi-domain polynomial (BDP) method [30].

Table 1
Dependence of the parameters λ and $\Omega(\lambda)$ on the indenter geometry. Below, ν represents the Poisson ratio, δ is the indentation depth, R is the indenter radius of flat cylinder and spherical geometries, and θ is the half-opening angle of conical indenter.

Geometry	λ	$\Omega(\lambda)$	contact radius
flat cylinder	1.0	$\frac{2R}{(1-\nu^2)}$	R
spherical	1.5	$\frac{4}{3}\frac{\sqrt{R}}{(1-\nu^2)}$	$\sqrt{R\delta}$
conical	2.0	$\frac{2}{\pi}\frac{\tan\theta}{(1-\nu^2)}$	$\delta\tan\theta$

3.2. Viscoelastic force model

Many nanoindentation force models have been developed in the last decade to study the viscoelastic properties of soft materials with the AFM, with particular emphasis on materials exhibiting power-law relaxation [5,7,26,31–33]. In contrast, different research groups independently developed similar models departing from fractional calculus [34] and the functional method of Lee and Radok [35].

The force-indentation relationship in time domain depends on the indentation history $\delta(t)$, as well as on intrinsic properties of the sample and can be described by the following expression [36]

$$F(t) = \Omega(\lambda)\int_0^t E(t-t')\frac{d\delta^\lambda(t')}{dt'}dt', \tag{3}$$

where $E(t)$ is the time-dependent relaxation function of the material. Recent studies have demonstrated that a linear indentation history accurately approximates a standard force curve's loading and unloading phases, closely mirroring experimental conditions [32,36]. This approximation is considered physically robust, as follows:

$$\delta(t) = \delta_{max}\begin{cases} t/t_l & 0 \le t \le t_l, \\ \left[(t_l+t_u)-t\right]/t_u & t_l < t \le t_l+t_u, \end{cases} \tag{4}$$

where t_l is loading time, and t_u is the unloading time.

The viscoelastic relaxation of living cells is most usually described as a single PL in the time domain [26,37]

$$E(t) = E_{ref}\left(\frac{t}{t_{ref}}\right)^{-\beta}, \tag{5}$$

where $E_{ref} = E(t_{ref})$ is a reference value of the elasticity modulus at an arbitrary scaling time, $t = t_{ref}$, and β is the relaxation exponent that lies in the range $0 \le \beta \le 1$, where $\beta = 0$ indicates a perfectly elastic sample, and $\beta = 1$ represents a Newtonian viscous fluid. Intermediate values of β hold both solid and fluid behaviors and hence are characteristic of power-law viscoelastic materials. The elasticity modulus at any given time t can be obtained with the scaling rule $E(t)t^\beta = E(t_{ref})t_{ref}^\beta$. In particular, we assume $t_{ref} = t_l$.

In a conventional AFM force curve, the load (l) and unload (u) curves are, respectively, given by

$$F_l(t) = \lambda\Omega(\lambda)B(\lambda, 1-\beta)E(t_l)\delta_{max}^\lambda\left(\frac{t}{t_l}\right)^{\lambda-\beta}, \tag{6}$$

$$F_u(t) = \lambda\Omega(\lambda)E(t_l)\delta_{max}^\lambda\left[B(\tau_l/t, \lambda, 1-\beta)\left(\frac{t}{t_l}\right)^{\lambda-\beta} - \frac{t_l^\beta}{t_u^\beta}\left(\frac{1}{1+\beta}\right)\left(\frac{t-t_l}{t_u}\right)^{1-\beta}{}_2F_1\left(1, 1-\lambda, 2+\beta; \frac{t-t_l}{t_u}\right)\right]. \tag{7}$$

$B(x;n,m)$ is the incomplete Beta function that obeys $B(n,m) = B(1;n,m)$, and $I(x;n,m) = B(x;n,m)/B(n,m)$ is the incomplete regularized Beta function, ${}_2F_1(a,b,c;x)$ is the Gauss hypergeometric function. Since all viscoelastic parameters are present in both loading and unloading parts, we focus our analysis in the loading curves because of its mathematical simplicity. Besides, one should notice that Eq. (6) can be written in different forms, revealing alternative ways to interpret it.

Method 1: In time domain, Eq. (6) can be written as

$$F_l(t) = F_{max}\left(\frac{t}{t_l}\right)^{\lambda-\beta}, \tag{8}$$

$$F_{max} = \lambda\Omega(\lambda)B(\lambda, 1-\beta)E(t_l)\delta_{max}^\lambda \tag{9}$$

where F_{max} is the maximum cantilever force in the end of the loading curve, which can be controlled by imposing a trigger force in the measurements. F_{max} depends on the indenter geometry, maximum indentation depth and loading time, and on the material

Table 2
Comparison of data extracted from the force curves shown in Figs. 2(a) and 2(d). The curves were fitted with HS and PL models. The parameter $v_\delta = \delta_{max}/t_l$ indicates the average indentation speed.

F_{max} (nN)	f_z (Hz)	t_l (s)	δ_{max} (μm)	v_δ (μm/s)	E_Y (kPa)	r^2_{HS}	$E(t_l)$ (kPa)	β	r^2_{PL}	$E_Y - E'_Y$ (kPa)
2	0.25	0.746	1.43	1.91	1.47	0.9446	1.04	0.198	0.9986	0.023
2	0.5	0.314	1.20	3.82	2.02	0.9935	1.50	0.176	0.9987	0.024
2	1.0	0.131	1.17	8.93	2.09	0.9984	1.55	0.175	0.9994	0.034
2	2.0	0.072	1.09	15.14	2.45	0.9980	1.70	0.208	0.9991	0.052
1	0.5	0.252	1.09	4.32	1.00	0.9799	0.77	0.152	0.9986	0.016
2	0.5	0.300	1.16	3.87	1.53	0.9938	0.87	0.303	0.9990	0.050
4	0.5	0.390	1.36	3.49	2.06	0.9985	1.42	0.210	0.9993	0.048
8	0.5	0.521	1.72	3.30	2.54	0.9883	1.77	0.207	0.9994	0.051

properties. In a log-log plot, the loading force curve obeys a power-law whose exponent directly shows the viscoelastic relaxation exponent, even if materials exhibit double PL relaxation [5].

Method 2: Combining Eqs. (4), (5) and (6) makes it possible to write the loading force in an HS-like form with a time-dependent Young's modulus $E_Y(t)$.

$$F_l[\delta(t)] = \Omega(\lambda) E_Y(t) \delta^\lambda(t), \tag{10}$$

$$E_Y(t) = \lambda B(\lambda, 1-\beta) E(t). \tag{11}$$

In the case of $\beta = 0$ the above equations recover the HS model for elastic materials, i.e., $E(t)$ is time-dependent. Equation (10) reveals an important detail which is normally overlooked when using HS model to study soft materials: the fitted value of E_Y will depend on the fitted range of the loading curve. Moreover, the Young's modulus is geometry-dependent and larger than the actual elasticity modulus by a factor of $E_Y(t)/E(t) = \lambda B(\lambda, 1-\beta)$. Since living cells are well represented by $\beta \approx 0.2$, this correction factor takes values of 1.39, 1.33 and 1.25 for conical, spherical and flat indenter geometries, respectively. Therefore, E_Y values measured with conical indenter must be 4.5% and 11% larger than the ones measured with spherical and flat indenters for the same material, while E_Y values measured with spherical indenters must be larger 6.5% than the ones measured with flat ones. Finally, due to the explicit time-dependence of $E_Y(t)$ in Eq. (10), the approximate relaxation function can be directly obtained from a single loading force curve by making

$$E(t) = \frac{F(t)}{\lambda \Omega(\lambda) B(\lambda, 1-\beta) \delta^\lambda(t)}. \tag{12}$$

Apart from the factor $B(\lambda, 1-\beta)$, the local viscoelastic relaxation can be directly obtained from the loading part of the AFM force curve.

4. Results

4.1. Simulated force curves

AFM force curves can be simulated departing from Eqs. (2) and (11). In regular force curves, the piezo actuator extends and retracts up to a maximum distance z_{ramp} according to $z(t) = z_i \mp v_z t$, where z_i is the initial piezo position, and the signal $\mp$ indicates whether the piezo is approaching to or moving away from the sample surface. The piezo extension rate v_z is related to the vertical scanning frequency f_z as $v_z = 2 z_{ramp} f_z$. When reaching an extension z_0 the AFM tip touches the sample surface (without deforming it, i.e., $\delta = 0$) while exhibiting a deflection d_0. For larger extensions ($z > z_0$), the AFM cantilever deflects upwards ($d > d_0$) as it indents the sample ($\delta > 0$). The piezo continues this movement until it reaches an extension (z_{max}) that produces a maximum cantilever deflection ($\Delta d_{max} = d_{max} - d_0$) corresponding to a maximum force applied $F_{max} = k_c \Delta d_{max}$. From this point, the piezo is retracted and the cantilever deflection is reduces until the AFM tip looses contact with the sample. This whole process is depicted in Fig. 1(a). The resulting simulated force curve is obtained by solving Eq. (2) to determine $d(t)$ for each t. As the parameters z_{ramp}, f_z and F_{max} are configured prior to measurements in the AFM software, in our simulations they also become input parameters.

Figs. 1(b) and 1(c) show simulated AFM force curves with different frequencies f_z and indenter geometries, subjected to $F_{max} = 2$ nN. The curves $F(z)$ clearly show that both f_z and tip geometry strongly affect the apparent Young's modulus of the samples. For a fixed f_z, the curve of the conical indenter yields the smallest Young's modulus, while measurements made with a flat cylinder the largest. This is in general justified in terms of contact area, which is smallest for the conical shape, and largest for the flat cylinder [24]. Besides, it has been shown analytically and numerically that conical indenters are less susceptible to finite thickness effects than other shapes [38]. A simple analysis of the HS model (Eq. (2)) shows that, for a fixed force, the larger is the contact area the smaller becomes the indentation depth, thereby yielding larger Young's modulus. This simple analysis is accurate for perfectly elastic samples. However, soft materials are intrinsically viscoelastic and the loading time becomes crucial. Fig. 1(d) shows that loading times of the force curves vary drastically for different f_z, and different indenter geometries. Thus, when probing viscoelastic materials

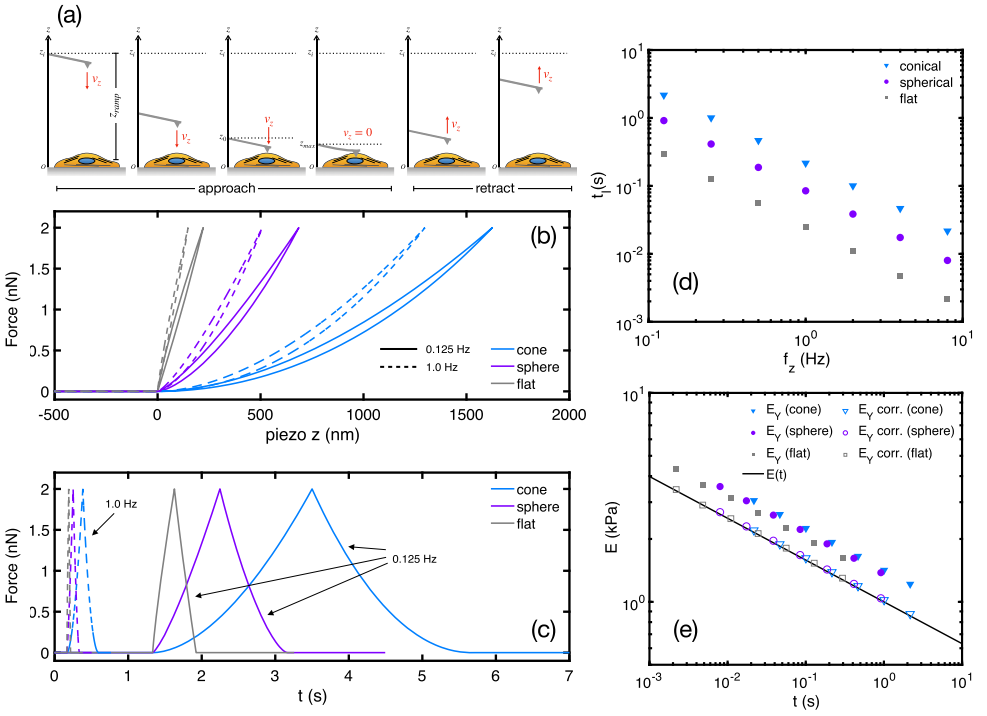

Fig. 1. (a) Schematics of the cantilever movement and deflection during a conventional AFM force curve. (b-c) Simulated AFM force curves of a power-law material ($E_{ref} = 1$ kPa, $t_{ref} = 1$ s, $\beta = 0.2$) measured with different f_z frequencies and indenter geometries as a function of the piezo displacement and time, respectively. The parameters used to generate these curves are $k_c = 0.06$ N/m, $z_{ramp} = 3$ μm, $R = 2.5$ μm (flat cylinder and spherical indenters), $\theta = 38^o$ (conical indenter). All force curves are subjected to a maximum trigger force of 2 nN. (d) Relationship between the loading time t_l of simulated force curves as a function f_z. (e) Comparison of the fitted (solid symbols) and corrected (open symbols) Young's moduli with the actual underlying power-law relaxation curve.

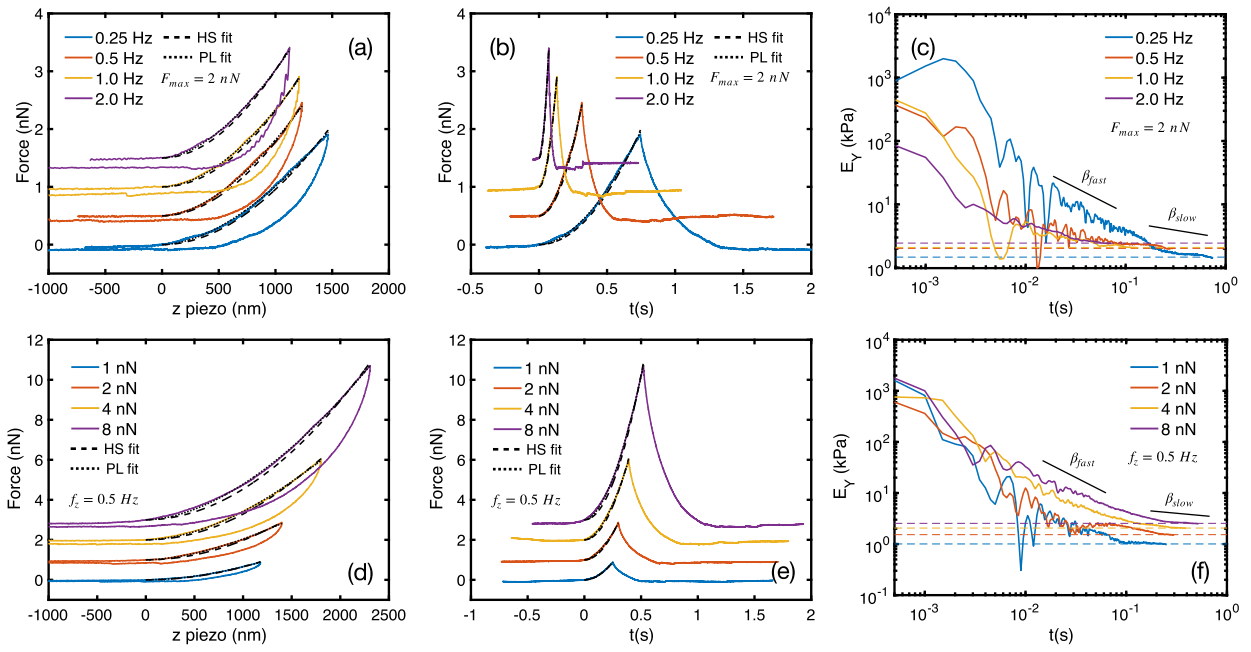

Fig. 2. AFM force curves of OFCOLII cells in two different loading conditions: (i) fixed F_{max} and varying f_z (panels a-c), and (ii) fixed f_z and varying F_{max} (panels d-f). For each loading condition, the curves were measured at the same site. The force curves are presented in $F(z)$ form in panels (a) and (d), and in the $F(t)$ form in panels (b) and (e). Curves are shifted vertically for better visualization and fitted with HS (dashed lines) and PL (dotted lines) models. The obtained parameters are listed in Table 2. Panels (c) and (f) represent the *time-dependent* Young's moduli given by $E_Y(t) = F(t)/[\Omega(\lambda)\delta^\lambda(t)]$. The horizontal dashed lines represent the fitted Young's moduli obtained with the HS model.

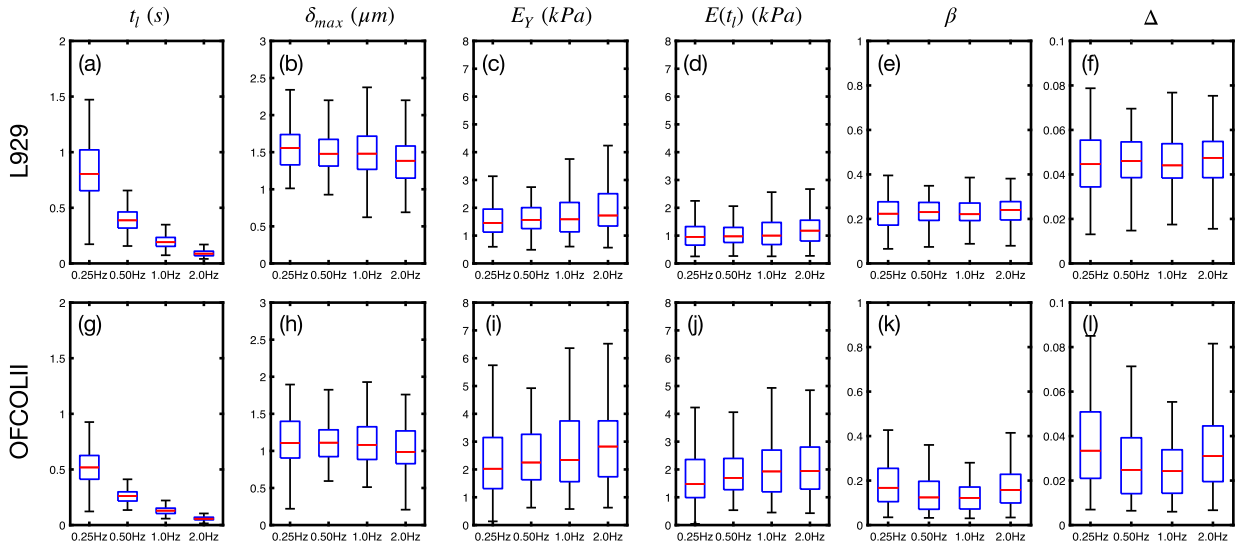

Fig. 3. Viscoelastic parameters of L929 and OFCOLII cells for $F_{max} = 2$ nN and varying $f_z = 0.25$, 0.5, 1.0 and 2.0 Hz, corresponding to piezo extension velocities of 1.5, 3.0, 6.0 and 12 μm/s, respectively. For each dataset, a total of $n_{L929} = 13$ and $n_{OFCOLII} = 16$ cells were probed, whereas 16 force curves per cell were measured. The quantity $\Delta = (E_Y - E'_Y)/E_Y$ describes the difference between HS and PL models.

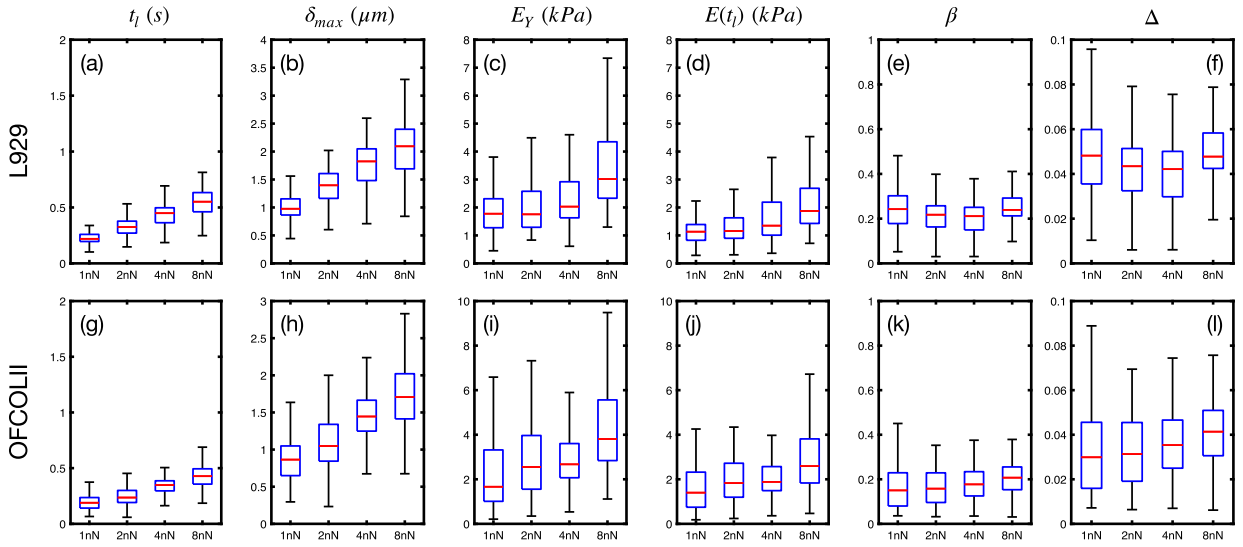

Fig. 4. Viscoelastic parameters of L929 and OFCOLII cells for f_z‘ = 0.5 Hz, corresponding to a piezo extension velocity of 3 μm/s, and varying forces $F_{max} = 1$, 2, 4 and 8 nN. For each dataset, a total of $n_{L929} = 15$ and $n_{OFCOLII} = 16$ cells were probed, whereas 16 force curves per cell were measured. The quantity $\Delta = (E_Y - E'_Y)/E_Y$ describes the difference between HS and PL models.

with the AFM, even when standardizing F_{max}, we are in fact probing not only different indentation depths, but also different loading times.

By varying f_z, while keeping a maximum force of 2 nN, we obtain loading times (t_l) ranging within two orders of magnitude (few ms to few seconds). Such a range is wide enough to reveal the relaxation properties of many types of soft samples. Furthermore, the curve $E_Y(t_l)$ differs from the actual relaxation function by a fixed factor such that $E_Y(t_l) = \lambda B(\lambda, 1-\beta)E(t_l)$, as shown in Fig. 1(e). Such a behavior is very robust and independent on the type indenter geometry. Finally, despite of the assumption of HS model to be valid only for purely elastic materials, by probing samples with wide enough range of f_z frequencies, we can reconstruct the underlying relaxation function of the samples.

4.2. Experimental force curves

Fig. 2(a) shows force curves measured in the same location of an OFCOLII osteoblast with fixed F_{max} and varying f_z. The hysteresis in the curves clearly shows the viscoelastic response of the cell. The fitted data in Table 2 show that, for a maximum

applied force of $F_{max} = 2$ nN, the increase of f_z from 0.25 Hz to 2 Hz reduces the loading times from 0.746 s to 0.072 s, and reduces the δ_{max} from 1.43 μm to 1.09 μm. In this range, the Young's moduli E_Y increased from 1.47 kPa to 2.45 kPa. The analysis with the PL model shows the increase of $E(t_l)$ from 1.04 kPa to 1.70 kPa, while the relaxation exponent fluctuates around $\beta \approx 0.2$, exhibiting little dependence on f_z. For all curves, the comparison between E_Y (from the HS model) with the effective Young's modulus $E'_Y = \lambda B(\lambda, 1-\beta)E(t_l)$ of the PL model shows a maximum difference of only 52 Pa. This is a strong experimental evidence of the connection between the time-dependent PL force and HS models.

Despite the good agreement between HS and PL models for fixed F_{max}, cells are known to exhibit nonlinear mechanical responses when subjected to increasing forces [28]. This makes one wonder whether this agreement is still valid for nonlinear deformation regimes. In this regard, Fig. 2(d) shows force curves measured with fixed $f_z = 0.5$ Hz and varying maximum forces from 1 nN to 8 nN. For such loading conditions, both t_l and δ_{max} increase with F_{max}, displaying an opposite trend with respect to the measurements with fixed F_{max}. The elasticity moduli E_Y and $E(t_l)$ also strongly increase with F_{max}, while β exhibits a slight increase tendency. Here, the comparison between models also exhibits a maximum difference of the order of 50 Pa, indicating that the agreement between models is also valid under nonlinear responses of the cells.

4.3. Intra- and inter-cell variability

The mechanical properties are very inhomogeneous over the cell surface. We performed AFM measurements in several cells of two different cell lines to address this issue. For each cell, we measured 16 force curves over a squared area of 4×4 μm^2, where each curve is fitted with both HS and PL models. The data for fixed F_{max} and varying f_z are shown in Fig. 3, and the data for fixed f_z and varying F_{max} in Fig. 4.

The increase of f_z, for fixed $F_{max} = 2$ nN, effectively increases the indentation velocity by reducing the loading times t_l. For the L929 cells, the frequencies of $f_z = 0.25, 0.5, 1.0, 2.0$ Hz yield average loading times of $t_l = 0.8, 0.4, 0.2, 0.1$ s. For the OFCOLII cells, the loading times are 25% smaller than the values obtained for the L929 cells. These measurement parameters result in approximate maximum indentation depths of $\delta_{max} = 1.5$ μm and $\delta_{max} = 1.1$ μm for L929 and OFCOLII cells, respectively. On average, the OFCOLII cells are roughly 30% stiffer than L929 ones. E_Y and $E(t_l)$ moduli exhibit a slight increase with f_z for both cell lines, while the relaxation exponents remain nearly constant. In both cell lines, the values of $E(t_l)$ are consistently smaller than E_Y, in agreement with Eq. (11). The exponents of OFCOLII cells are lower than of L929 cells, indicating that L929 cells exhibit an increased fluid character compared to OFCOLII cells. The comparison of E_Y with the effective Young's modulus E'_Y shows that both models differ by less than 5% for both cell lines. Finally, the boxplots of Fig. 3 exhibit dispersion in all measured parameters. For example, Young's moduli show a dispersion of the order of 1 kPa between the 1st and 3rd quartile for the curves measured with $f_z = 1$ Hz. This is caused by the variability of stiffness of over the cell surface and between cells [31].

Concerning the response of the cells for increasing forces, t_l and δ_{max} increase in both cell lines. Forces of 8 nN produce maximum indentation depths of 2.1 μm and 1.7 μm in L929 and OFCOLII cells, respectively. Consequently, OFCOLII cells are stiffer than L929 cells for larger external forces. Interestingly, both E_Y and $E(t_l)$ moduli increase non-linearly with F_{max}. This varying elasticity modulus is due to the nonlinear mechanical stiffening of the cells [28]. On the other hand, the trends of the relaxation exponents β seem to be cell-dependent, exhibiting a slight reduction for L929 cells, and increase for OFCOLII cells. Finally, the comparison of the effective E'_Y and actual E_Y Young's moduli shows that these quantities differ, on average, by up to 5% even when the cells are subjected to nonlinear deformation responses.

We also performed the data analysis above, fixing $\delta_{max} = 0.5$ μm for varying f_z for both cells (See Supplementary Material). For shallow indentation depths, which are just a bit larger than the thickness of the cell cortex, the average values of t_l are much shorter than the ones of Fig. 3, resulting in larger values of $E(t_l)$ and E_Y. Again, we obtained differences between E'_Y and actual E_Y of approximately 70 Pa, confirming that our effective Young's modulus obtained from the PL model is also valid for fixed δ_{max}.

4.4. Determining $E(t)$ from a single force curve

Equation (11) shows that fitting a force curve $F(t)$ versus $\delta(t)$ using the HS model provides a sort of *time-dependent* $E_Y(t)$ where t is the time duration that the AFM tip takes, departing from the contact point, to achieve an indentation depth of $\delta(t)$. Such an approach has been previously employed to obtain a depth-dependent $E_Y(\delta)$ without formal proof, as the one provided in our study. The same approach has also been proposed as a mechanical tomography method to probe the interior of cells [39]. The *time-dependent* Young's modulus $E_Y(t)$ of the force curves measured in Figs. 2(a) and 2(d) are shown in Figs. 2(c) and 2(f), respectively. The constructed $E_Y(t)$ curves for different f_z are very similar exhibiting two relaxation regimes, a fast relaxation regime (up to 200 ms) with exponent β_{fast}, and a slow relaxation regime for larger observation times with exponent β_{slow} ($\beta_{fast} > \beta_{slow}$). These two relaxation regimes have been observed in many reports in both time and frequency domains [5,40–42]. Evidence of the fast relaxation regime was also found in the analysis for fixed $\delta_{max} = 0.5$ μm (see Supplementary Material). The measured values of t_l are roughly a few tens of milliseconds, depending on f_z, thereby within the fast relaxation timescales. The fitting of the loading force curves for such shallow indentations resulted in relaxation exponents more than 50% larger than those obtained for force curves with $\delta_{max} > 1$ μm (see Fig. 3).

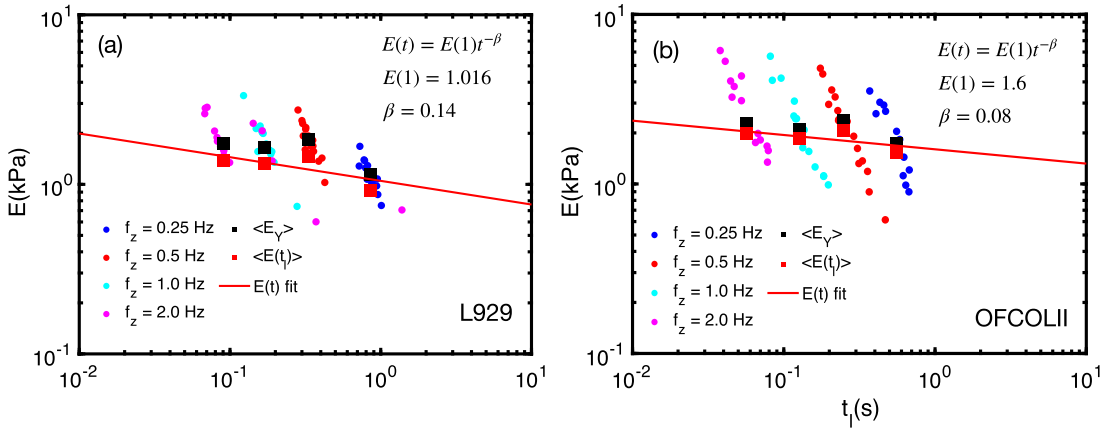

Fig. 5. Construction of the relaxation function $E(t)$ for a single cell by performing multiple measurements over an area of 16 μm^2 with varying f_z frequencies. Each curve is fitted with HS model to obtain $\langle E_Y \rangle$ *versus* $\langle t_l \rangle$ data points, which can be fitted with $\langle E_Y \rangle = A\langle t_l \rangle^{-\beta'}$, where β' is the average relaxation exponent of the cell, and $A = \lambda B(\lambda, 1-\beta')E(1)$, where $E(1)$ is the actual elasticity modulus of the cell at $t = 1$ s.

4.5. Determining $E(t)$ with HS model

With the connection between the Young's modulus of the HS model with the time-dependent PL force model of cells proved, the natural question that arises is how to determine the actual viscoelastic relaxation function $E(t)$ using only HS model, given the mechanical inhomogeneities over a whole cell and their nonlinear mechanical response.

Due to the linear relationship between E_Y and $E(t)$ (Eq. (11)), one can construct $E(t)$ for a single (or a collection of cells) by measuring those cells with the largest possible range of f_z. According to Fig. 3, keeping F_{max} constant, we can explore the mechanical properties of cells at different times t_l that may approximately range from 10^{-2} s to 10^0 s by changing f_z from 0.25 Hz to 2 Hz. This range can be enlarged from 0.1 Hz to 10 Hz in most AFM setups, providing the possibility of exploring the relaxation properties of cells over two orders of magnitude in time (from tens of milliseconds to a few seconds).

We measured 16 force curves over a squared area of 4×4 μm^2 of side of a single cell of each cell line. Each curve is fitted with the HS model, and the data points of $E_Y(t_l)$, depicted in Fig. 5, clearly shows the dispersion of E_Y and t_l, due to the inhomogeneous properties of different sites of the cell surface. The dependence of the average $\langle E_Y \rangle$ with the average $\langle t_l \rangle$, represented by the large black squares, exhibits a power-law-like behavior which, according to Eq. (11), should exhibit the same time dependence of the viscoelastic relaxation function $E(t)$ given by Eq. (5). Fitting those data points with $\langle E_Y \rangle = A\langle t_l \rangle^{-\beta'}$, resulted in $\beta' = 0.14$ and $A = 1.6$ for the OFCOLII cell. A direct comparison of this fitting function with Eqs. (5) and (11) shows that (i) the exponent β' can be regarded as an average relaxation exponent of the measured cell, (b) the parameter $A = \lambda B(\lambda, 1-\beta')E(1)$ is proportional to the average cell elasticity modulus $E(1)$ at $t_{ref} = 1$ s, whereas the whole cell is considered an homogeneous viscoelastic body.

4.6. Validity of the linear indentation profile

Our viscoelastic force model departed from a linear indentation profile assumption in the loading/unloading curves. We tested the validity of this assumption in our measurements by modeling the experimental indentation curves as $\delta(t) = \delta_{max}(t/t_l)^n$, where deviations from $n = 1$ represent nonlinear indentation profiles. These data are shown in the Supplementary Material. For small forces of 2 nN, we obtain average values ranging between $n = 0.98$ and $n = 1.0$ for both L929 and OFCOLII cells, despite of the cantilever speed (f_z). For increasing forces up to 8 nN, the average values range between $n = 0.97$ and $n = 0.99$, with the OFCOLII cells exhibiting a slightly larger nonlinearity than the L929 cells. Such tiny reductions in the exponent n do not represent a significant deviation from the linear indentation assumption of Eq. (4). These results are in line with the analytical solution of the indentation profile for power-law materials of Brückner et al. [32], which shows that for moderate combination of cantilever speeds and spring constant, the linear indentation profile is a good approximation. Moreover, as shown in the Supplementary Material, the nonlinear form of the indentation profile keeps the analytical form of Eq. (11) and, consequently the relationship between HS and our power-law force model. The only difference is a slight change in Young's modulus that becomes $E_Y(t) = n\lambda B(n\lambda, 1-\beta)E(t)$.

4.7. Indenter geometry effects

Several studies reported large variations in the Young's moduli of cells measured with different indenter geometries [24,25,43–45]. Among those, the works of Kulkarni et al. [24] and Chiou et al. [25] stand out because they studied the effect of three different geometries (conical/pyramidal, spherical and flat) at different loading conditions. All those studies found the same trend, i. e., $E_Y^{cone} > E_Y^{sphere} > E_Y^{cylinder}$ for the same cell type. This comparative trend agrees qualitatively, but not quantitatively, with our model. For instance, Chiou et al. found that $E_Y^{cone}/E_Y^{sphere} \approx 2$, $E_Y^{cone}/E_Y^{flat} \approx 2$ and $E_Y^{sphere}/E_Y^{flat} \approx 1$. Similar ratios were also found by the

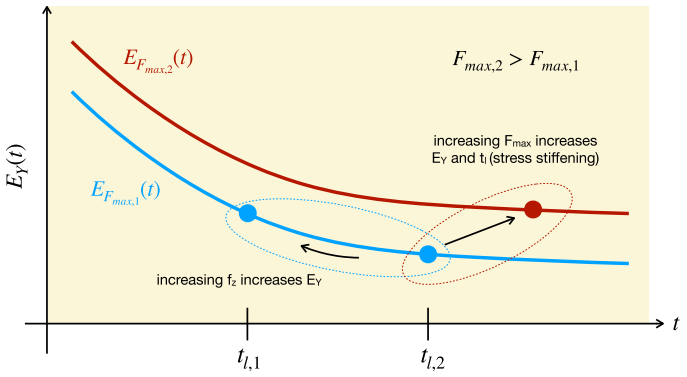

Fig. 6. Diagram showing how the measurement parameters $f_z \propto t_l^{-1}$ and F_{max} influence the fitted Young's modulus E_Y in PL viscoelastic materials. The solid lines represent the *time-dependent* Young's modulus ($E_Y(t) \propto E(t)$), while the points represent the fitted Young's modulus for a specific combination of parameters f_z and F_{max}.

other mentioned works. Comparatively, Eq. (11) predicts that $E_Y^{cone}/E_Y^{sphere} = 1.045$, $E_Y^{cone}/E_Y^{flat} = 1.11$ and $E_Y^{sphere}/E_Y^{flat} = 1.065$, assuming $\beta = 0.2$ and given that E_Y is measured with different geometries and identical timescales.

The variation of the Young's modulus measured with different indenter geometries is often justified only in terms of the different contact radius (see Table 1) that leads to non-uniform contact pressure distribution below the indenter. According to Kulkarni et al., it is preferable to compare the mechanical properties of cells at comparable average pressure. Since this is very hard to achieve, they standardized a maximum indentation depth of $\delta_{max} = 0.4$ μm to compare E_Y measured with different geometries. Differently from Kulkarni, Chiou standardized F_{max} to compare data.

Although none of the above works included time in their analyzes, time is implicitly embedded in the measurements. We have simulated force curves in a cell using the measurement parameters (indenter geometry, cantilever speed and spring constant) from Chious's work (see Supplementary Material). We found that standardizing F_{max} does not lead to standardization of t_l. Fixing $F_{max} = 1nN$, we obtained $t_l^{cone} > t_l^{sphere} > t_l^{flat}$ where $t_l^{cone}/t_l^{sphere} \approx 4.6$ and $t_l^{cone}/t_l^{flat} \approx 14.5$. Consequently, comparing E_Y measured with different indenters in the same cell is equivalent to compare the mechanical properties of the cell at different relaxation timescales. Thereby, it is reasonable that the ratios of E_Y be different from the predictions of our model. On the other hand, standardizing $\delta_{max} = 0.4$ μm nearly leads to the standardization of t_l. We obtained $t_l^{cone} < t_l^{sphere} < t_l^{flat}$, where $t_l^{cone}/t_l^{sphere} \approx 0.87$, $t_l^{cone}/t_l^{sphere} \approx 0.75$ and $t_l^{sphere}/t_l^{flat} \approx 0.87$. For such a condition, the ratio E_Y^{cone}/E_Y^{sphere} is raised to 1.074, as compared to 1.045 predicted by our model. However, this ratio still is much below the measurements of Kulkarni et al. who also found $E_Y^{cone}/E_Y^{sphere} \approx 2$.

One of the possible reasons for such a increased ratio is that sharp conical/pyramidal tips are very sensitive to small scale cytoskeleton fibers (e.g. actin bundles and microtubules) whose stiffness is of the order of GPa as compared to the average stiffness of the cell body of few kPa [28]. On the other hand, indenters with large radii (spherical/flat) are much less sensitive to small scale stiffer areas and only feel an averaged mechanical response of the cytoskeleton components and cytoplasm [24]. Other factor that may affect the measurements of E_Y with different geometries is that indenters with large contact radius are more susceptible to finite thickness effects, such that indentation depths larger that 10% of the sample thickness should be avoided, or properly treated with a viscoelastic force model that takes into account the finite thickness effects [38,46].

5. Discussion

As a general rule, the fitting of the force curves with the HS model exhibits slightly worse goodness-of-fit parameters r^2 when compared to the PL force model because a constant value of E_Y cannot account for the time-dependent relaxation of the elasticity modulus during the loading curve. However, this poor fitting can be mitigated by performing faster force curves (increasing f_z), for which the relaxation amplitude is smaller than for slow force curves, as shown in Table 2 for fixed F_{max}. On the other hand, one cannot increase f_z too much because the drag resistance on the cantilever increases. In this case, the fluid drag must be considered in the force model. For instance, reference [31] shows a method to remove the drag contribution to the force curve, but it requires additional calibration steps to the measurements workflow. Alternatively, Efremov et al. developed a numerical postprocessing protocol to remove the drag contribution that can be applied to extremely fast force curves like the ones in fast force mapping and Peakforce Tapping AFM modes [45].

The use of HS model results in Young's moduli strongly dependent on the parameters adopted in the measurement, namely the vertical frequency f_z and maximum trigger force F_{max}. Both parameters determine the duration t_l of the loading curve, which is the timescale for the underlying viscoelastic processes. In fact, the PL force model shows that E_Y is proportional to the actual elasticity modulus $E(t)$ at $t = t_l$ (see Eq. (11)). Therefore, one can construct the approximate relaxation function $E(t)$ by exploring the inter-dependence of t_l, f_z and F_{max} in multiple force curves.

The values of E_Y for different measurement parameters must qualitatively represent the behavior of the underlying relaxation function. For instance, the increase of E_Y with f_z for fixed F_{max} reflects the high elasticity moduli of materials at very short timescales, while measurements with large f_z reflect the lower elasticity moduli at large timescales. This qualitative model to

Table 3
Comparison between our model and Efremov's model calculated by Eq. (15).

ϕ	$\beta = 0$	$\beta = 0.1$	$\beta = 0.2$	$\beta = 0.4$	$\beta = 0.6$
$\gamma = 2$ ($t_u = t_l$)					
$\lambda = 1$	1	0.933	0.871	0.758	0.660
$\lambda = 1.5$	1	0.960	0.924	0.860	0.809
$\lambda = 2$	1	0.928	0.967	0.947	0.942
$\gamma = 1.8$ ($t_u = 0.8t_l$)					
$\lambda = 1$	1	0.923	0.852	0.727	0.619
$\lambda = 1.5$	1	0.950	0.905	0.825	0.759
$\lambda = 2$	1	0.972	0.947	0.908	0.885

describe how the AFM measurement parameters affect the fitted elasticity modulus is schematically shown in Fig. 6. Since f_z is inversely proportional to both t_l and δ_{max}, such a behavior is predicted by Eq. (9), which can be used for quick estimates of $E(t_l)$. Moreover, HS model is also able to study the nonlinear response of the cells when subjected to increasing forces.

The proposed method to construct the viscoelastic relaxation function departing from several measurements of E_Y at different timescales t_l can be extended to more challenging scenarios, like (i) using blunted cone indenter model to describe pyramidal tips more realistically [43,47], and (ii) for large indentation depths using either flat or spherical indenters, which are very susceptible to finite thickness effects [38,48], and the force curves must be fitted with a thickness-corrected elastic model [46].

Efremov et al. have previously investigated the relationship between E_Y and $E(t)$ [33]. They have numerically shown that the apparent E_Y, determined in the whole indentation cycle duration $T_{cycle} = t_l + t_u$, is close to the time-averaged value of the $E(t)$ within the limits of the indentation cycle regardless of the indenter geometry and relaxation function, i.e.,

$$E_Y \approx \langle E \rangle = \frac{1}{0.25T_{cycle}} \int_0^{0.25T_{cycle}} E(t)dt. \tag{13}$$

For elastic samples, one has $t_u = t_l$, and for viscoelastic samples $t_u < t_l$. Thus, we can write $T_{cycle} = \gamma t_l$ ($1 \leq \gamma \leq 2$) to represent elastic ($\gamma = 2$) and viscoelastic materials ($1 \leq \gamma < 2$). Solving this integral using Eq. (5), we obtain:

$$\bar{E}_Y \approx \langle E \rangle = \frac{(0.25\gamma)^{-\beta}}{(1-\beta)} E(t_l). \tag{14}$$

We can compare our model with Efremov's by calculating the ratio

$$\phi = \frac{E_Y(t_l)}{\bar{E}_Y} = \lambda B(\lambda, 1-\beta)(1-\beta)(0.25\gamma)^{\beta}, \tag{15}$$

whose results are shown in Table 3. The data show that Efremov's model is similar to our model in the two cases: (i) low viscoelastic exponents, regardless the indenter geometry, and (ii) for conical indenters, regardless the viscoelastic exponent.

6. Conclusions

In this work, we demonstrated how fitting AFM force curves with the Hertz-Sneddon (HS) model can be used to study the viscoelastic response of power-law viscoelastic soft materials. More specifically, we showed how to quantify the viscoelastic properties of living cells, which obey complex power-law relaxation, obtained from the widely adopted framework of the HS model. This data analysis protocol can be rapidly incorporated into the routine biomechanical characterization of cells and other soft materials, and it can be easily adapted to study materials that obey other types of viscoelastic relaxation. By incorporating the viscoelastic nature of samples and the other standardization protocol proposed by Perez-Dominguez et al. [23], we finally established the pathway to turn biomechanics into a metrology-graded method for biomedical engineering applications.

CRediT authorship contribution statement

I.V.M. Lima: Writing – original draft, Methodology, Formal analysis, Conceptualization. **A.V.S. Silva:** Methodology, Data curation. **F.D. Sousa:** Validation, Methodology. **W.P. Ferreira:** Methodology, Formal analysis. **R.S. Freire:** Methodology. **C.L.N. de Oliveira:** Writing – original draft, Conceptualization. **J.S. de Sousa:** Validation, Methodology.

Declaration of competing interest

The authors declare that they have no known competing financial interests or personal relationships that could have appeared to influence the work reported in this paper.

Data availability

All data that support the findings of this study are included within the article and in the supplementary material.

Acknowledgements

This work was supported by the Brazilian agencies CNPq, CAPES and FUNCAP, and by Fundação Edson Queiroz.

Appendix A. Supplementary material

Supplementary material related to this article can be found online at https://doi.org/10.1016/j.heliyon.2024.e30623.

References

[1] C. Rotsch, M. Radmacher, Drug-induced changes of cytoskeletal structure and mechanics in fibroblasts: an atomic force microscopy study, Biophys. J. 78 (Jan. 2000) 520–535.
[2] B. Fabry, L. Buscemi, M. Grabulosa, X. Trepat, B. Fabry, R. Farré, D. Navajas, Microrheology of human lung epithelial cells measured by atomic force microscopy, Biophys. J. 84 (2003) 2071.
[3] L.M. Rebelo, J.S. de Sousa, J. Mendes Filho, M. Radmacher, Comparison of the viscoelastic properties of cells from different kidney cancer phenotypes measured with atomic force microscopy, Nanotechnology 24 (2012) 055102.
[4] B. Han, H.T. Nia, C. Wang, P. Chandrasekaran, Q. Li, D.R. Chery, H. Li, A.J. Grodzinsky, L. Han, Afm-nanomechanical test: an interdisciplinary tool that links the understanding of cartilage and meniscus biomechanics, osteoarthritis degeneration, and tissue engineering, ACS Biomater. Sci. Eng. 3 (Aug. 2017) 2033–2049.
[5] J.S. de Sousa, F.R.S.F.D. Sousa, M. Radmacher, A.F.B. Silva, M.V. Ramos, A.C.O. Monteiro-Moreira, F.P. Mesquita, M.E.A. Moraes, R.C. Montenegro, C.L.N. Oliveira, Double power-law viscoelastic relaxation of living cells encodes motility trends, Sci. Rep. 10 (2020) 4749.
[6] R. Garcia, Nanomechanical mapping of soft materials with the atomic force microscope: methods, theory and applications, Chem. Soc. Rev. 49 (2020) 5850.
[7] P.D. Garcia, C.R. Guerrero, R. Garcia, Nanorheology of living cells measured by afm-based force–distance curves, Nanoscale 12 (2020) 9133.
[8] I. Sneddon, The relation between load and penetration in the axisymmetric Boussinesq problem for a punch of arbitrary profile, Int. J. Eng. Sci. 3 (1965) 47.
[9] S.E. Cross, Y.-S. Jin, J. Tondre, R. Wong, J. Rao, J.K. Gimzewski, Afm-based analysis of human metastatic cancer cells, Nanotechnology 19 (Aug. 2008) 384003.
[10] A. Stylianou, T. Stylianopoulos, Atomic force microscopy probing of cancer cells and tumor microenvironment components, BioNanoScience 6 (Dec. 2015) 33–46.
[11] M. Lekka, Discrimination between normal and cancerous cells using afm, BioNanoScience 6 (2016) 65.
[12] A. Stylianou, M. Lekka, T. Stylianopoulos, Afm assessing of nanomechanical fingerprints for cancer early diagnosis and classification: from single cell to tissue level, Nanoscale 10 (45) (2018) 20930–20945.
[13] M. Plodinec, M. Loparic, C.A. Monnier, E.C. Obermann, R. Zanetti-Dallenbach, P. Oertle, J.T. Hyotyla, U. Aebi, M. Bentires-Alj, R.Y.H. Lim, C.-A. Schoenenberger, The nanomechanical signature of breast cancer, Nat. Nanotechnol. 7 (2012) 757.
[14] E. Darling, S. Zauscher, F. Guilak, Viscoelastic properties of zonal articular chondrocytes measured by atomic force microscopy, Osteoarthr. Cartil. 14 (June 2006) 571–579.
[15] M. Stolz, R. Gottardi, R. Raiteri, S. Miot, I. Martin, R. Imer, U. Staufer, A. Raducanu, M. Düggelin, W. Baschong, A.U. Daniels, N.F. Friederich, A. Aszodi, U. Aebi, Early detection of aging cartilage and osteoarthritis in mice and patient samples using atomic force microscopy, Nat. Nanotechnol. 4 (Feb. 2009) 186–192.
[16] Z. Chang, L. Zhang, J.-T. Hang, W. Liu, G.-K. Xu, Viscoelastic multiscale mechanical indexes for assessing liver fibrosis and treatment outcomes, Nano Lett. 23 (Oct. 2023) 9618–9625.
[17] S. Pérez-Domínguez, J. López-Alonso, F. Lafont, M. Radmacher, Comparison of rheological properties of healthy versus dupuytren fibroblasts when treated with a cell contraction inhibitor by atomic force microscope, Int. J. Mol. Sci. 24 (Jan. 2023) 2043.
[18] Z. Chang, J. Zhang, Y. Liu, H. Gao, G.-K. Xu, New mechanical markers for tracking the progression of myocardial infarction, Nano Lett. 23 (Aug. 2023) 7350–7357.
[19] C. Rianna, M. Radmacher, Influence of microenvironment topography and stiffness on the mechanics and motility of normal and cancer renal cells, Nanoscale 9 (2017) 11222.
[20] C. Rianna, M. Radmacher, S. Kumar, Direct evidence that tumor cells soften when navigating confined spaces, Mol. Biol. Cell 31 (July 2020) 1726–1734.
[21] D. Rudoy, S.G. Yuen, R.D. Howe, P.J. Wolfe, Bayesian change-point analysis for atomic force microscopy and soft material indentation, J. R. Stat. Soc., Ser. C, Appl. Stat. 59 (June 2010) 573–593.
[22] N. Gavara, Combined strategies for optimal detection of the contact point in afm force-indentation curves obtained on thin samples and adherent cells, Sci. Rep. 6 (2016) 21267.
[23] S. Pérez-Domínguez, S.G. Kulkarni, J. Pabijan, K. Gnanachandran, H. Holuigue, M. Eroles, E. Lorenc, M. Berardi, N. Antonovaite, M.L. Marini, J. Lopez Alonso, L. Redonto-Morata, V. Dupres, S. Janel, S. Acharya, J. Otero, D. Navajas, K. Bielawski, H. Schillers, F. Lafont, F. Rico, A. Podestà, M. Radmacher, M. Lekka, Reliable, standardized measurements for cell mechanical properties, Nanoscale 15 (40) (2023) 16371–16380.
[24] S.G. Kulkarni, S. Pérez-Domínguez, M. Radmacher, Influence of cantilever tip geometry and contact model on AFM elasticity measurement of cells, J. Mol. Recognit. 36 (7) (2023) e3018.
[25] Y.-W. Chiou, H.-K. Lin, M.-J. Tang, H.-H. Lin, M.-L. Yeh, The influence of physical and physiological cues on atomic force microscopy-based cell stiffness assessment, PLoS ONE 8 (Oct. 2013) e77384.
[26] V.G. Gisbert, F.M. Espinosa, J.G. Sanchez, M.C. Serrano, R. Garcia, Nanorheology and nanoindentation revealed a softening and an increased viscous fluidity of adherent mammalian cells upon increasing the frequency, Small (Sept. 2023).
[27] M.A. Caporizzo, C.M. Roco, M.C.C. Ferrer, M.E. Grady, E. Parrish, D.M. Eckmann, R.J. Composto, Strain-rate dependence of elastic modulus reveals silver nanoparticle induced cytotoxicity, Nanobiomedicine 2 (Jan. 2015) 9.
[28] P. Kollmannsberger, B. Fabry, Linear and nonlinear rheology of living cells, Annu. Rev. Mater. Res. 41 (2011) 75.
[29] R. Benítez, S. Moreno-flores, V.J. Bolós, J.L. Toca-Herrera, A new automatic contact point detection algorithm for AFM force curves, Microsc. Res. Tech. 76 (June 2013) 870–876.
[30] R. Roy, J.P. Desai, Determination of mechanical properties of spatially heterogeneous breast tissue specimens using contact mode atomic force microscopy (afm), Ann. Biomed. Eng. 42 (2014) 1806.
[31] F.M. Hecht, J. Rheinlaender, N. Schierbaum, W.H. Goldmann, B. Fabry, T.E. Schäffer, Imaging viscoelastic properties of live cells by afm: power-law rheology on the nanoscale, Soft Matter 11 (2015) 4584.
[32] B.R. Brückner, H. Nöding, A. Janshoff, Viscoelastic properties of confluent mdck ii cells obtained from force cycle experiments, Biophys. J. 112 (Feb. 2017) 724–735.

[33] Y.M. Efremov, S.L. Kotova, P.S. Timashev, Viscoelasticity in simple indentation-cycle experiments: a computational study, Sci. Rep. 10 (Aug. 2020) 13302.
[34] A. Jaishankar, G.H. McKinley, Power-law rheology in the bulk and at the interface: quasi-properties and fractional constitutive equations, Proc. R. Soc. A 469 (2012) 20120284.
[35] E.H. Lee, J.R.M. Radok, The contact problem for viscoelastic bodies, J. Appl. Mech. 27 (Sept. 1960) 438–444.
[36] J.S. de Sousa, J.A.C. Santos, E.B. Barros, L.M.R. Alencar, W.T. Cruz, M.V. Ramos, J.M. Filho, Analytical model of atomic-force-microscopy force curves in viscoelastic materials exhibiting power law relaxation, J. Appl. Phys. 121 (2017) 034901.
[37] A.L.D. Moura, W.V. Santos, F.D. Sousa, R.S. Freire, C.L.N. de Oliveira, J.S. de Sousa, Viscoelastic relaxation of fibroblasts over stiff polyacrylamide gels by atomic force microscopy, Nano Express 4 (Sept. 2023) 035008.
[38] D.F.S. Costa, J.L.B. de Araújo, C.L.N. Oliveira, J.S. de Sousa, Nanoindentation in finite thickness viscoelastic materials, J. Appl. Phys. 132 (Dec. 2022) 214701.
[39] C. Roduit, S. Sekatski, G. Dietler, S. Catsicas, F. Lafont, S. Kasas, Stiffness tomography by atomic force microscopy, Biophys. J. 97 (July 2009) 674–677.
[40] L. Deng, X. Trepat, J.P. Butler, E. Millet, K.G. Morgan, D.A. Weitz, J.J. Fredberg, Fast and slow dynamics of the cytoskeleton, Nat. Mater. 5 (2006) 636.
[41] B.D. Hoffman, G. Massiera, K.M. Van Citters, J.C. Crocker, The consensus mechanics of cultured mammalian cells, Proc. Natl. Acad. Sci. USA 103 (2006) 10259.
[42] B.D. Hoffman, J.C. Crocker, Scaling cell mechanics: dissecting the physical responses of cells to force, Annu. Rev. Biomed. Eng. 11 (2009) 259.
[43] F. Rico, P. Roca-Cusachs, N. Gavara, R. Farré, M. Rotger, D. Navajas, Probing mechanical properties of living cells by atomic force microscopy with blunted pyramidal cantilever tips, Phys. Rev. E 72 (Aug. 2005).
[44] P. Carl, H. Schillers, Elasticity measurement of living cells with an atomic force microscope: data acquisition and processing, Pflügers Arch. Eur. J. Physiol. 457 (May 2008) 551–559.
[45] Y.M. Efremov, A.I. Shpichka, S.L. Kotova, P.S. Timashev, Viscoelastic mapping of cells based on fast force volume and peakforce tapping, Soft Matter 15 (27) (2019) 5455–5463.
[46] P.D. Garcia, R. Garcia, Determination of the elastic moduli of a single cell cultured on a rigid support by force microscopy, Biophys. J. 114 (June 2018) 2923–2932.
[47] S. Kontomaris, A. Malamou, A. Stylianou, The hertzian theory in afm nanoindentation experiments regarding biological samples: overcoming limitations in data processing, Micron 155 (Apr. 2022) 103228.
[48] S.V. Kontomaris, A. Malamou, A novel approximate method to calculate the force applied on an elastic half space by a rigid sphere, Eur. J. Phys. 42 (Feb. 2021) 025010.